Journal Pre-proof

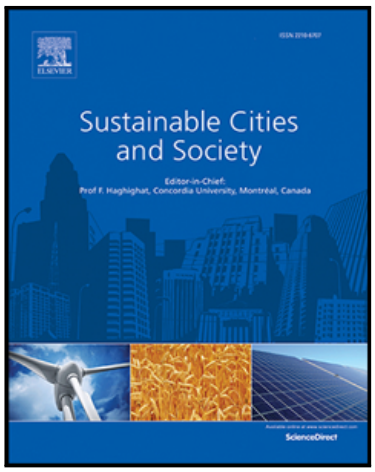

On the mitigation potential of higher urban albedo in a temperate oceanic metropolis

Serena Falasca , Michele Zinzi , Lan Ding , Gabriele Curci , Mattheos Santamouris

PII: S2210-6707(22)00177-9
DOI: https://doi.org/10.1016/j.scs.2022.103850
Reference: SCS 103850

To appear in: *Sustainable Cities and Society*

Received date: 28 December 2021
Revised date: 16 February 2022
Accepted date: 16 March 2022

Please cite this article as: Serena Falasca , Michele Zinzi , Lan Ding , Gabriele Curci , Mattheos Santamouris , On the mitigation potential of higher urban albedo in a temperate oceanic metropolis, *Sustainable Cities and Society* (2022), doi: https://doi.org/10.1016/j.scs.2022.103850

On the mitigation potential of higher urban albedo in a temperate oceanic metropolis

Serena Falasca[1,2,3,*], Michele Zinzi[4], Lan Ding[5], Gabriele Curci[1,2], Mattheos Santamouris[5]

1. Department of Physical and Chemical Sciences, University of L'Aquila, Via Vetoio, 67100 Coppito - L'Aquila, Italy

2. Center of Excellence for the Remote Sensing and Forecast of Severe Weather (CETEMPS), Department of Physical and Chemical Sciences, University of L'Aquila, Via Vetoio, 67100 Coppito - L'Aquila, Italy

3. Now at Department of Physics, Sapienza University of Rome, Piazzale Aldo Moro 5, 00185 Rome, Italy

4. ENEA-Italian National Agency for New Technologies, Energy and Sustainable Economic Development, Via Anguillarese 301, 00123 Rome, Italy

5. Faculty of Built Environment, University of New South Wales, Sydney, NSW 2052, Australia

*Corresponding Author:

Serena Falasca, Department of Physics, Sapienza University of Rome, Piazzale Aldo Moro 5, 00185 Rome, Italy

E-mail address: serena.falasca@uniroma1.it

Serena Falasca: serena.falasca@uniroma1.it

Michele Zinzi: michele.zinzi@enea.it

Lan Ding: lan.ding@unsw.edu.au

Gabriele Curci: gabriele.curci@univaq.it

Mattheos Santamouris: m.santamouris@unsw.edu.au

Highlights:

- ¶ High resolution modeling of a whole metropolis with 0.5x0.5 km^2 grid
- ¶ Detailed urban land use classification based on ten Local Climate Zones
- ¶ 1.4°C maximum of air temperature drop for 0.27 increase of city albedo
- ¶ 260 m maximum of planetary boundary layer height drop for 0.27 increase of city albedo

Abstract: The urban overheating calls for the implementation of mitigation actions. The article aims at demonstrating the advantages and the risks associated with the increase of the city albedo in Melbourne (Australia), through high resolution numerical analyses based on a detailed urban land use. The Weather Research and Forecasting model was used to calculate the spatial and temporal local climate change for three increased albedo scenarios and three different urban densities. In the scenario with highest albedo, the ambient temperature decreases of about 1.6°C in the middle and high density zones and 0.9°C in the low density zones. The sea breeze extends the thermal benefit due to the albedo increase to non-urban areas, despite it is slightly weakened by the diminished land-sea temperature contrast. The pollutant levels are expected to increase, due to a combination of slower winds (drops up to 0.19 ms^{-1}) and decreased planetary boundary layer heights (drops from 175 m up to 291 m). High and low density classes have the highest and lowest risk of stagnation, respectively. Due to the contrasting results in terms of thermal mitigation and pollution risks, the study calls for the identification of comprehensive metrics to asses optimal values of urban albedo.

Keywords: urban heat mitigation; high albedo; WRF; WUDAPT; BEP; Melbourne

1. Introduction

Urban heat island is an extremely documented phenomenon in more than 400 cities all around the world; it deals with higher ambient temperatures in the dense parts of the cities compared to their surrounding environment (Akbari et al., 2015). The phenomenon is caused by the positive thermal balance in the urban built environment mainly because of the excessive absorption of solar radiation by the construction surfaces, the release of anthropogenic heat, the reduced evapotranspiration and surface permeability, and the lack of urban ventilation (Santamouris and Chrisomalidou, 2001). The intensity of urban overheating may range up to 10°C, however, its magnitude is highly intensified during heat wave periods as result of the important energetic synergy between the local and global climate change (Santamouris, 2015; Founda and Santamouris, 2017; Khan et al., 2021; Ciancio et al., 2020). Higher urban temperatures cause a serious impact on human life: increase the energy use and peak electricity for cooling purposes, affect indoor and outdoor thermal comfort, affect the survivability levels of low income population, rise the concentration of harmful pollutants and in particular of the ground level ozone, reduce the efficiency of power generation plants and increase the levels of heat related mortality and morbidity (Arrieta et al., 2005; Santamouris, 2014a; Santamouris et al., 2015; Santamouris, 2020). Exposure to high ambient temperatures affects the human thermoregulation system and causes important heat related health problems and mortality risk (Johnson et al., 2005; Gosling et al., 2009; Schinasi et al., 2018). The phenomenon, finally, has a serious and negative impact on low income population (Santamouris and Kolokotsa, 2015).

Urban mitigation technologies aim to decrease the heat gains and enhance the heat losses in cities and involve the use of advanced materials for the building skin and the urban surfaces, the use of additional greenery, as well as the dissipation of the excess urban heat in low temperature heat sinks (Santamouris et al., 2017). Reviews on the available technical solutions are provided by Croce and Vettorato, 2021 and Shooshtarian et al., 2018. Several studies have evaluated the cooling

potential of modified albedo urban scenarios using different modeling techniques (Santamouris 2014b; Alchapar and Correa, 2016; Falasca et al., 2019; Tsoka et al., 2018), as well as large-scale urban projects (Santamouris and Yun, 2020). Microscale analyses are also carried out to evaluate the local impact in limited areas of a city (Dimoudi et al., 2014; Peron et al., 2015). Furthermore, studied applications concern different urban surfaces, such as roofs (Xu et al., 2012) and roads (Carnielo and Zinzi, 2013) also in combination with other mitigation techniques (Shahidan et al., 2012; Taleghani et al., 2014; Salata et al., 2017). As it concerns the impact of modified albedo on health, it is found that it may reduce in average heat related mortality by 19.8 % per degree of temperature drop, or 1.8 % per 0.1 increase of the albedo (Santamouris and Fiorito, 2021).

There is a considerable lack of knowledge on the cooling potential and the associated impact on the urban climate of reflective materials in coastal cities strongly influenced by the advection of hot air from desert zones. Previous studies have shown the effectiveness of high albedo materials in mitigating urban thermal stress in Melbourne (Coutts et al., 2013) and nowadays greater attention to the implications on atmospheric circulation and air quality is essential. The emerging ozone pollution in Australian cities (Ryan et al. 2021) and the smoke-related emissions of recent Australian fires are two potential targets of such implications (Johnston et al., 2021). Pearce et al., (2011) highlighted the relative importance of weather variables affected by the highly reflective materials (i.e., temperature, wind speed intensity, radiation) on the regional air pollution in Melbourne.

Through the case of the city of Melbourne (Australia), this study aims at deepening the understanding of the way the increase of the albedo affects the local climate beyond the mere temperature reduction in coastal cities impacted by desert advections climatic phenomena. This task requires to analyze the different components of the thermal balance in the city and to quantify the potential positive and negative effects of the albedo modification, so that

comprehensive information may fruitfully drive the successful implementation of reflective materials at city scale.

2. Materials and method

The methodology consists of the following successive steps:

- identification of the current city land use as a function of the main categories (greenery, roads and pavements, roofs, other) and reference radiative properties of the used urban materials
- selection of three different and progressive scenarios of increased albedo of urban materials
- development of the numerical model and validation versus observations
- simulation and comparison of the four different scenarios.

The key performance indicators selected to express the cooling potential of the materials with increased albedo and their impact on the urban local climate are: air and surface temperature, wind speed, sensible and latent heat fluxes, the height of the Planetary Boundary Layer (hereinafter, PBLH). The sensible and latent heat fluxes (included in the surface energy balance) and the surface temperature are the driver of near surface variables, such as air temperature, wind speed and PBLH.

To be noted that the modification of the urban albedo may influence the energy performance of buildings, because of the increased solar gains though windows and walls due to the reflected shortwave radiation, as documented in previous studies (Xu et al., 2020; Qin, 2015). This aspect, however, was not taken into account, since no sufficient details on installed air conditioning systems were available to process further analyses about the relation between the local air

temperature and the modification anthropogenic heat sources, induced by different albedo values.

2.1. The city: Melbourne, AU

The city of Melbourne is the capital of Victoria State, in the south-east of Australia, and the second most populous city in the country. The urban area has an extension of about 2.450 km^2, while the entire metropolitan area, known as Greater Melbourne, has an extension close to 10,000 km^2 and a population of 5 million inhabitants. The city alternates densely built area, as the central commercial district (19500 inhabitants per square kilometres), and green areas, ranging from small neighbourhood parks to urban forest. Melbourne is classified *Cfb* according to the Köppen-Geiger climate classification, which means temperate oceanic climate with warm to hot summers and mild winters. As a coastal city, Melbourne is affected by the sea-land breeze. This type of local circulation implies a diurnal rotation, with the wind blowing from the sea towards the city during the daytime and from the city towards the sea during the night (Stull, 1988). As demonstrated by several numerical and observational studies (e.g., Freitas et al., 2007; Shen et al., 2018), the circulation associated with the urban heat island enhances the air flow from regions surrounding the urban area. In the case of Melbourne, advection of hot air is observed in Melbourne from the evening to the early morning, due to the presence of the desert north of the city.

2.2. The scenarios for albedo variants

Different albedo scenarios are implemented to the urban surfaces most stressed by the solar radiation: buildings' roofs and pavements; the latter including all the built urban surfaces: roads, squares, sidewalks, parking lot, pedestrian areas, etc. The different configurations have

progressive increase of albedo values compared to the reference case: the first scenario (S1) doubles the initial albedo values of roofs and pavements; 0.1 and 0.2 progressive increases of pavement and roof albedo, respectively, are implemented for S2 and S3. Such increments are applied to the totality of the related urban surfaces. In order to provide realistic scenarios coherent with the current technologies, products available on the market easily meet the albedo values considered for the analysis, and the quantities are reported in Table 1. The albedo of not constructed surfaces (e.g. green area, bare land, etc.) is assumed 0.2 for all the scenarios.

Table 1. Albedo of urban fabrics for the reference case and the scenarios.

Urban fabric	albedo [-]			
	Reference	S1	S2	S3
Road/pavement	0.15	0.3	0.4	0.5
Roof	0.20	0.4	0.6	0.8

3. Calculation

3.1. Modelling

In this study, the Weather Research and Forecasting modeling system (WRF, version 4.1.2) is applied to reproduce the meteorological fields over the urban area of Melbourne. The simulated period spans from 1st January to 28th February 2019. Four two-way nested domains are simulated with a horizontal resolution increasing from 13.5 km in the largest domain (d01) to 0.5 km in the innermost domain covering the urban area of Melbourne (d04), with a constant grid ratio equal to 3 (Table 1S). The geographical areas covered by the domains are shown in Figure 1. The vertical grid is equal for the four domains, consisting in 33 total levels and 10 levels in the 1000 m from the ground. The physics options characterizing the WRF configuration are listed in Table 2S. Initial and

global boundary conditions are the final operational global analysis data of the National Center for Environmental Prediction, with a spatial resolution of 0.25°×0.25° and a temporal resolution of 6 hours (NCEP, 2015). Land use and soil types for the simulated areas are provided by the United States Geological Survey (USGS) dataset, together with the WUDAPT database for the detailed categorization of urban classes (see Section 3.3). For more details on the model, the reader is referred to the technical notes (Skamarock et al., 2019) and the Users' Guide (https://www2.mmm.ucar.edu/wrf/users/docs/user_guide_v4/).

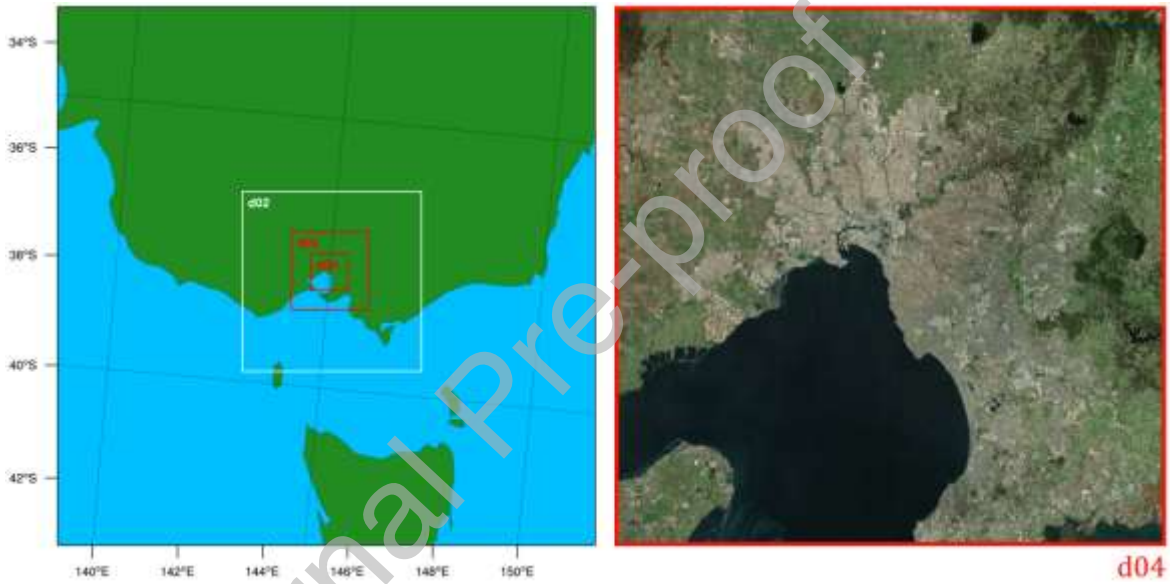

Figure 1. On the left, the four two-way nested WRF domains over Melbourne. On the right, satellite image of the innermost domain.

3.2. The city model

The city model is integrated in WRF through a Multi-layer urban canopy parameterization, namely the Building Effect Parameterization (BEP) (Martilli et al., 2002). Information about the morphology of Melbourne is supplied by the World Urban Database Access Portal Tool (WUDAPT, https://www.wudapt.org/). Such project (Ching et al., 2018) led also to the implementation of WUDAPT into the WRF model, based on the lowest level of WUDAPT detail (level 0) that labels the cities areas in terms of Local Climate Zone (LCZ) types according to the classification by Stewart

and Oke (2012) and Stewart, Oke and Krayenhoff (2014) (Brousse et al., 2016; Martilli et al., 2016). In WRF, WUDAPT considers ten LCZ types corresponding to ten urban classes characterized by different values of thermal and morphological properties. In the LCZ map of Melbourne (Figure 2), only the following six urban classes are present: compact high-rise, compact midrise, compact low rise, open low rise, large low rise, sparsely built. The features of such urban classes are detailed in Table 2; the urban fraction expresses the portion of the urban class that does not have natural vegetation. The designed scenarios (Table 1) have been implemented by modifying the values of the albedo for roofs and roads for all the urban classes, while keeping the default values of the other urban thermal properties (e.g., heat capacity, thermal conductivity). The validation of the model is included in the Supplementary material. Correlation coefficients are consistent with findings by Ribeiro et al. (Ribeiro et al., 2021) for another seaside city, Barcelona. The ability of WRF-BEP configurations to correctly reproduce the day-night rotation of the breeze in a coastal site in Italy was also demonstrated in (Falasca et al., 2021b). The features of such urban classes are detailed in Table 2; the urban fraction expresses the portion of the urban class that does not have natural vegetation.

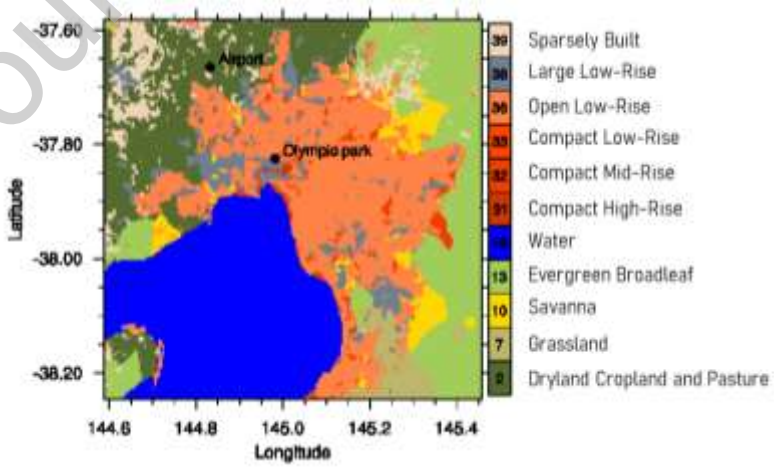

Figure 2. Land use classes in the innermost domain according to the WUDAPT database. Markers show the location of the weather stations of the Australian Bureau of Meteorology.

Table 2. Features of the urban texture present in the Melbourne Local Climatic Zone (LCZ) map.

Urban class	Texture	Street width [m]	Building width [m]	Building height [m]	Pavement area [%]	Roof area [%]	Green area [%]
31	Compact high rise	15	15	27.25	75	25	0
32	Compact midrise	12.7	17.5	12.25	63	32	5
33	Compact low rise	5.7	9	7.25	57	33	10
36	Open low rise	12.4	10.5	6.75	51	14	35
38	Large low rise	32.5	28.8	8.25	66	19	15
39	Sparsely built	10	10	6.25	23	8	70

Starting from the urban geometry as described in Table 2, the average albedo for each urban class is calculated, two values are provided: *a* is the albedo of the whole area (including greenery, bare soil, etc.), a_{cons} is the albedo of the constructed surfaces only. The specific classes are then grouped in three larger classes to compare the results against previous studies. These classes are aggregated according to the construction density: high (31+32+33), medium (36+38) and low (39). The correspondent albedo values are calculated using the area extension of each urban class as weight factor and the city average albedo is finally calculated (Table 3). To be noted that the average albedo variations among the urban classes do not follow a clear trend because of the different mix of roofs, pavement and green areas in each class, as inferred from Table 2.

Table 3. Average albedo as a function of the urban density, and mitigation scenario. *a* is the albedo of the whole surfaces, a_{cons} refers only to the constructed surfaces (green areas are excluded)

Urban density	Reference		Scenario 1		Scenario 2		Scenario 3	
	a_{cons} [-]	a [-]	a_{cons} [-]	a [-]	a_{cons} [-]	a [-]	a_{cons} [-]	a [-]
High	0.167	0.169	0.334	0.327	0.467	0.454	0.601	0.581
Medium	0.161	0.173	0.321	0.283	0.442	0.367	0.564	0.450
Low	0.163	0.189	0.325	0.238	0.450	0.275	0.575	0.313
City	0.16	0.17	0.32	0.28	0.44	0.36	0.57	0.44

4. Results and discussion

The analysis of the results follows the classification of High Density (hereinafter, HD), Middle Density (hereinafter, MD) and Low Density (hereinafter, LD) urbanization, taking into account spatial variation and temporal evolution. The air temperature and the wind speed are provided by WRF at 2 and 10 meters heights, respectively.

4.1. Insights from the reference case

The dissimilar features of the urban texture of the three urban density classes (see Tables 2 and 3) affect the terms of the surface energy balance (i.e., sensible and latent heat flux, radiation), and then the net flux at the ground determining the state of the overlying planetary boundary layer. Figure 3S shows the average daily cycles of the analyzed quantities for the three levels of urbanization in the reference case, together with the values averaged over the whole urban area.

The sensible heat flux is maximum in the HD class and minimum in the LD class throughout the entire daily cycle and the opposite condition characterizes the latent heat flux. In particular, for the latent heat flux the ratio between the peak values in LD and HD is more than 5. This behavior could be expected as the urban green fraction of LD is 70%, while it ranges from 0 to 10% in HD (Table 2). The surface temperature exhibits lower difference among the three categories in

comparison with the heat fluxes during the central hours of the day. It is observed that that the peak surface temperature is higher in LD (36°C) than in HD (33.8°C), the behavior can be explained by the shading projected by buildings in urban canyons, which limit the solar irradiation penetration in the high density built areas. The role of the urban morphology in shaping these phenomena, especially in summer months, is already documented in the existing literature (Andreou 2014). The ambient temperature is mostly lower that the surface temperature, with a delta close to 10°C between for peak values. The initial values range from 18.5°C of the LD to 19.2°C of the HD, while the initial average value is equal to about 18.8°C. During the night and the early morning, LD and HD are the coolest and hottest categories, respectively, while MD is characterized by the highest ambient temperature during the central hours of the day. This reveals that HD has a lower day-night temperature excursion than the other classes. Indeed, due to the greater thermal inertia of urban surfaces during the night, the ambient air cools down less than other two categories. Consistently with the surface temperature, PBLH reaches higher values in LD than in HD during the central hours of the day. Probably, in LD the more open surfaces and the fewer obstacles (like buildings) enhance the soil-atmosphere energy exchange driving the atmospheric boundary layer development. During the night the PBL is thicker in HD (371 m at midnight) than in LD (300 m at midnight) due to the higher thermal inertia of densely built neighborhoods as pointed out for the ambient temperature. The effect of urbanization density is evident on wind intensity, which is lower for areas characterized by higher urbanization density (see Figure 3S).

4.2. Spatial analysis of the impact of reflective materials

The spatial distributions (but not the magnitudes) of the reference case – scenario difference for the variables are comparable for the three scenarios. In order to avoid redundancy, only the intermediate S2 is shown in the main manuscript, corresponding images for S1 and S3 are included

in the Supplementary material. The discussion on the spatial distributions in S2 can be extended to the other scenarios. Particular attention in the investigation is given to the early morning (i.e., at 06:00 LT) and afternoon (i.e., at 14:00 LT) since they represent the minimum and peak conditions for the solar radiation. The white areas in the maps represent water, i.e. ocean and lakes.

4.2.1. Early morning conditions (06:00 LT)

The difference between the reference case and the scenarios is almost negligible for all the variables considered in this study. This is graphically confirmed by the coloring of the maps of the scenario-reference case difference is nearly uniform over the entire domain (Figure 3).

The sensible heat flux decreases by few units (about 4-5 Wm^{-2}) for all the scenarios. The maximum temperature decrease is 0.58°C in S3 and 0.24°C in S2, whereas the maximum average temperature is about 25°C in the reference case. Also the maximum drops of other variables are very low compared to the maximum values in the reference case. As an example, the maximum wind speed decrease is 0.19 m/s for S3 and the maximum average value in the reference case is about 4 m/s. Similarly, the maximum PBLH drop is around 30 m for all three scenarios, with an average peak value of about 1300 m in the reference case. Based on these amounts, it can be stated that at 06:00 LT the modification of albedo values has negligible effect on the thermal and dynamic fields. The indirect effect due to the reduced daytime cooling of the surfaces is weak. The results show that the advection of hot air from the desert (usual for this time) is not affected by the use of high albedo materials.

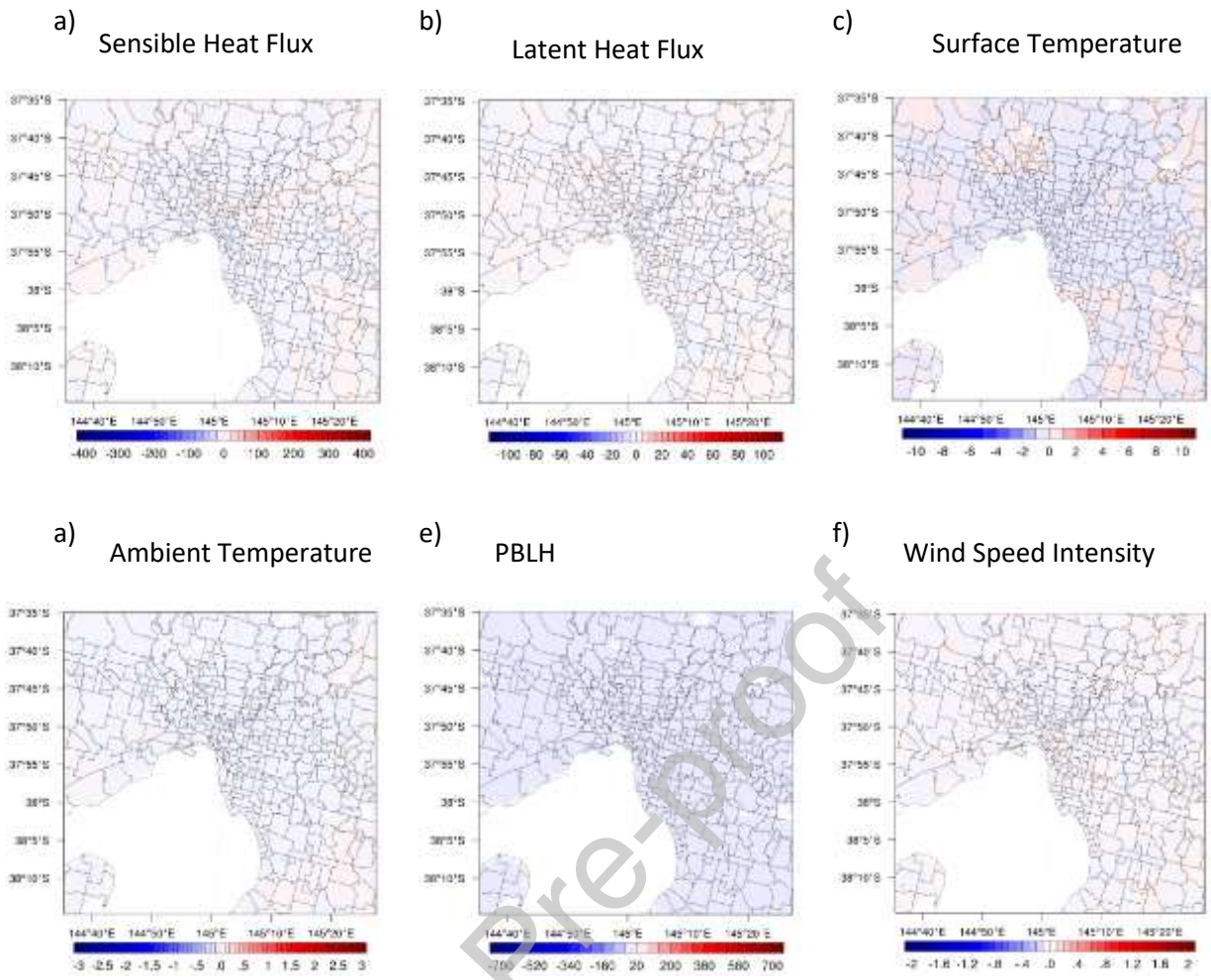

Figure 3. Spatial distribution of the difference between the S2 case and the reference case for: (a) sensible heat flux, (b) latent heat flux, (c) surface temperature, (d) ambient temperature, (e) planetary boundary layer height and (f) wind speed intensity at 06:00 LT.

4.2.2. Peak conditions (14:00 LT)

Figure 4a-f presents the spatial distribution of the S2-reference case differences at the peak hour for the quantities analyzes in this work. The maximum punctual decrease in sensible heat flux (equal to 225 Wm^{-2}) corresponds to a decrease of 5.5°C and 1.7°C in surface and ambient temperature, respectively. In the other scenarios, the local peak decreases of sensible heat flux of 323 Wm^{-2} and (S3) 127 Wm^{-2} (S1) correspond to ambient temperature drops of 2.6°C (S3) and 0.94°C (S1). For the latent heat flux, the difference with respect to the reference case exhibits a significant spatial unevenness, since in the western part of the city it decreases less compared to

the rest of the city. This area is surrounded by forests which contribute to increase the latent heat flux, partly neutralizing the role of high albedo materials. It should be also highlighted that the maps of heat fluxes and surface temperature (surface quantities) display a low density built-up area in the north-west corner of the domain where surface variables drop less than in the main urban area (MD and HD). This phenomenon is due to: i) the smaller extension of the surfaces covered by high albedo materials (with a consequent lower overall albedo, see Table 3) and ii) the presence of surrounding non-urban cells. Furthermore, the maps of sensible heat flux and surface temperature indicate an evident dissimilar coloring of the urban areas compared to the surrounding rural areas, corresponding exactly to the area where albedo is altered. The ambient temperature and PBLH reduction in magnitude is more gradual at the boundary between urban and rural areas, stressing the role of local atmospheric dynamics in addition to the surface thermal forcing. This phenomenon is more pronounced in the central hours of the day when the sea breeze blowing from the sea to the hinterland is stronger. This type of circulation mitigates hot summer days, especially in large metropolitan areas affected by strong urban heat island such as Melbourne (Imran et al., 2018; Jacobs et al., 2018). High albedo materials reduce locally the intensity of wind speed, also due to the drop of surface temperature – sea temperature driving the sea breeze (Epstein et al., 2017). Such drops imply a decline in the benefit of the breeze, especially in the cells closest to the coast. The reduction of wind intensity due to the highly reflective materials can facilitate stagnation conditions, with negative repercussion on pollutants dispersion and pedestrians comfort. In this case, the reduction of the diurnal sea breeze intensity is also crucial since it can transport pollutants outward the city during daytime. On the other hand, nighttime winds from North are not touched (see previous section). Air quality is worsened further by the reduction of the PBL, i.e. the part of the troposphere where pollutants accumulate. Our

simulations report decreases in the PBLH equal to 205.6 m, 367.4 m and 518.4 m for S1, S2 and S3 with respect to a PBLH equal to 1294.6 m in the reference case.

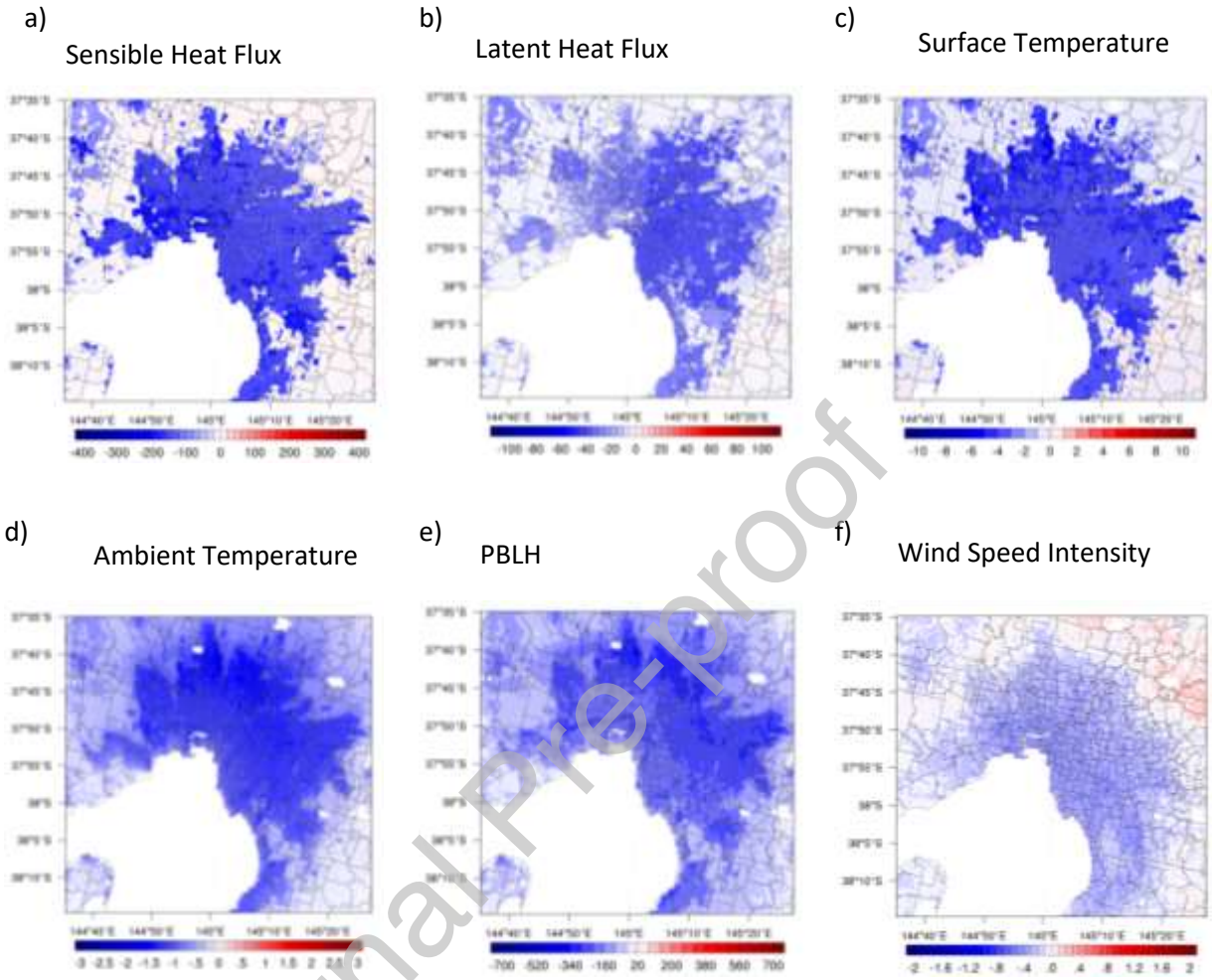

Figure 4. Same as Figure 3, but at 14:00 LT.

4.3. Temporal analysis of the mitigation potential for scenarios and urbanization classes

In this section, the results are illustrated for each quantity in terms of the daily evolution of the difference between the reference case and the three mitigation scenarios.

4.3.1. Surface variables

Figure 5 presents the average diurnal variation of the difference between the reference case and the scenarios S1, S2 and S3 for the surface variables (sensible and latent heat flux and the surface temperature) in the three urbanization classes. The differences increase during the morning up to

the peak at 14:00 LT for all the variables, then decrease to zero at night. Furthermore, for sensible heat flux and surface temperature alterations increase with the level of urbanization and with the albedo value, so that differences (black plots in Figure 5) are equal to 204 Wm^{-2} for S3, 140 Wm^{-2} for S2 and 74 Wm^{-2} for the average sensible heat flux in S1. This is consistent with the nature of the mitigation technique adopted in this study. The reductions in sensible heat flux for MD are closer to HD ones than to LD ones. The temporal evolution of the latent heat flux differences is analogous to those of the other surface variables. However, HD experiences lower reduction values compared to the other two classes since it is characterized by a lower fraction of vegetation (i.e., 1.44 Wm^{-2}, about 2.85 Wm^{-2} and 4.32 Wm^{-2} for the three scenarios). The MD class is characterized by the highest differences, with peak values more than double of the corresponding values in HD (i.e. 15 Wm^{-2}, 29 Wm^{-2} and 43 Wm^{-2} for S1, S2 and S3). Average values in Table 3S confirm that MD is affected by the highest reductions compared to the reference case. As for the sensible heat flux, the surface temperature drops less in LD than in MD and HD compared to the reference case. The urban structure and the consequent value of the overall albedo certainly contribute to this. However, the features of the neighboring areas could also have an effect in this, as discussed with regard to the spatial analysis. Indeed, grid cells surrounding LD are forests and therefore are not affected by the albedo materials. Contrarily, HD is completely surrounded by MD grid cells where there is a thermal drop for high albedo materials. Concerning the differences among the scenarios, average values are less than 1°C for all three density categories in S1, while they reach and exceed 1°C in S2 and grow further in S3 reaching an average value of 2.095°C (Table 6S). It is also worth noting that for the surface temperature nighttime drops are slightly higher than zero in S3. For example, the temperature drops to 5% of that amounts at 14:00 LT, while for sensible heat flux this percentage is insignificant. This can be interpreted as a sort of

memory of surfaces that involves a thermal benefit even at night, when the solar radiation is absent.

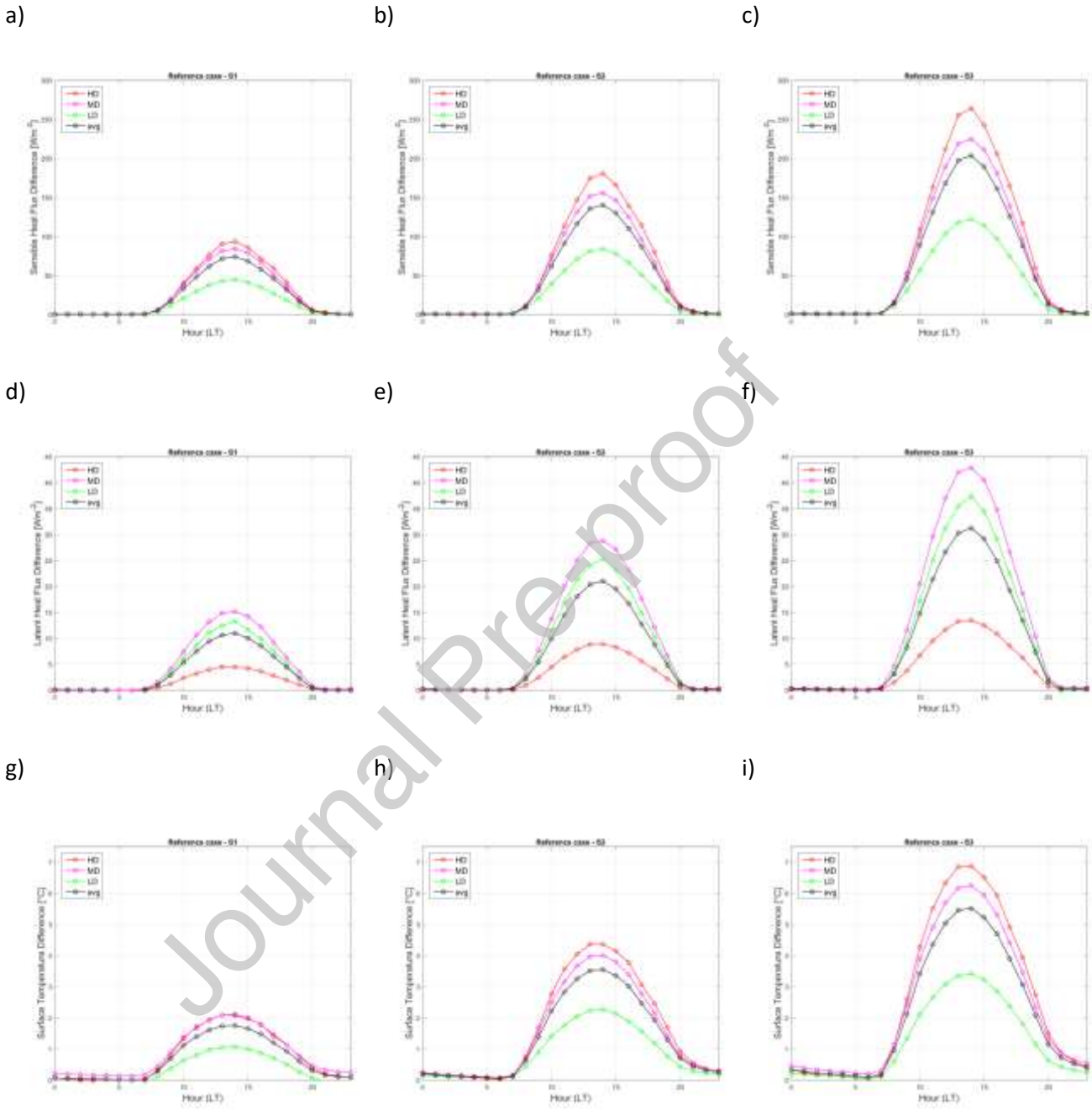

Figure 5. Average daily cycles of the differences between the reference case and the scenarios S1 (first column), S2 (second column) and S3 (third column) for the sensible heat flux (first row), the latent heat fluxe (second row) and the surface temperature (third row) for the three urbanization classes HD (red), MD (magenta) and LD (green). The black line represents the mean between the three density classes.

4.3.2. Near surface variables and PBLH

Since the decrease in surface temperature and sensible heat flux is higher for HD than for MD cells, one would expect the same for ambient temperature. Instead, the ambient temperature decrease for HD and MD cell is essentially the same in all the scenarios (Figure 6). More in detail, peak values (at 14:00 LT) are 1.6°C for MD and HD and 0.9°C for LD in S3, 1°C for MD and HD and 0.6°C in S2, 0.5°C for MD and HD and 0.3°C for LD in S1. This can have multiple reasons: i) the role of the breeze spreading the cooling effect of high albedo materials (i.e., from HD to MD), ii) HD grid cells are enclosed by MD zones, therefore the former can be influenced by the second that increase their temperature. We could define this phenomenon, described also above, as a "boundary effect", iii) the greater extension of urban surfaces in HD is balanced by the effects linked to the urban canyons (i.e., self-shading, multiple reflections of solar radiation).

Coastal areas (mainly MD) present a higher drop in wind speed intensity than the rest of the metropolitan area, consistently with the comments in the previous section. Values of average drops are very close for HD and MD, while they are about half for LD. For example, the average drops for S2 are equal to 0.124 ms^{-1} and 0.126 ms^{-1} for HD and MD and 0.0611 ms^{-1} for LD (Table 8S). The HD class has the maximum intensity decrease in the scenarios implying the highest stagnation risk, since it has the lowest wind intensity in the reference case. The LD class is characterized, instead, by the lowest wind intensity in the reference case throughout the day and has the least decrease in the scenarios. The three classes of urbanization have also different temporal evolutions of the wind speed (Figure 6). In fact, the maximum drop occurs in the central hours of the day (i.e., around 15:00 LT) for MD and HD, while it occurs in the evening (i.e., around 19:00 LT) for the LD class. Since the development of the wind speed intensity is similar for the three classes in the reference case, it can be inferred that this may depend on the geometrical/morphological features of the low density class that modify the daily cycle in the scenarios. It is interesting that the wind speed maximum decrease occurring in the afternoon for

LD makes this category less subject to pedestrian discomfort conditions for pedestrians than HD and MD, since ventilation reduction does not coincide temporally with thermal and radiative peaks. High albedo materials do not significantly influence the direction of the wind, which remains essentially from the sea. The average daily cycles of the PBLH in (Figure 6g-i and Table 9S) show a progressive strengthening of the effect of high albedo materials from scenario S1 to scenario S3. While HD and MD present quite same ambient temperature decreases for all the scenarios, PBLH drops are higher in MD than in HD, especially in S2 and S3. Regarding this, it should be noted that in MD a significant reduction of the mechanical forcing (similar decreases of wind speed intensity in HD and MD) is added to the reduction of the surface thermal forcing (higher in HD than in MD), both contributing to a lower vertical development of the PBL. As for temperature and wind speed, LD is characterized by a much lower drop of PBLH compared to the other classes. However, HD and MD manifest a double relative fall in PBLH compared to the reference case (in the reference case PBL is thicker in LD than in HD), with a consequent higher risk of degradation of the air quality. Moreover, the use of high albedo materials amplifies reflections of solar radiation enhancing the photochemical reactions of surface ozone production. And severe ozone events are often associated to thermo-hygrometric discomfort for pedestrians (Falasca et al., 2021a). Nevertheless, the LD graph presents a less steep descent than the other classes after 14:00 LT (especially in S1), implying a longer lasting of the reduction of PBLH (of its consequences as well, such as poor mixing) in LD than in MH and HD, although with lower magnitudes of the reductions. For example, in S1 decreases are close to 50 m from 13:00 LT to 17:00 LT for LD, while for HD and MD the values change significantly from one hour to the next in the central hours of the day.

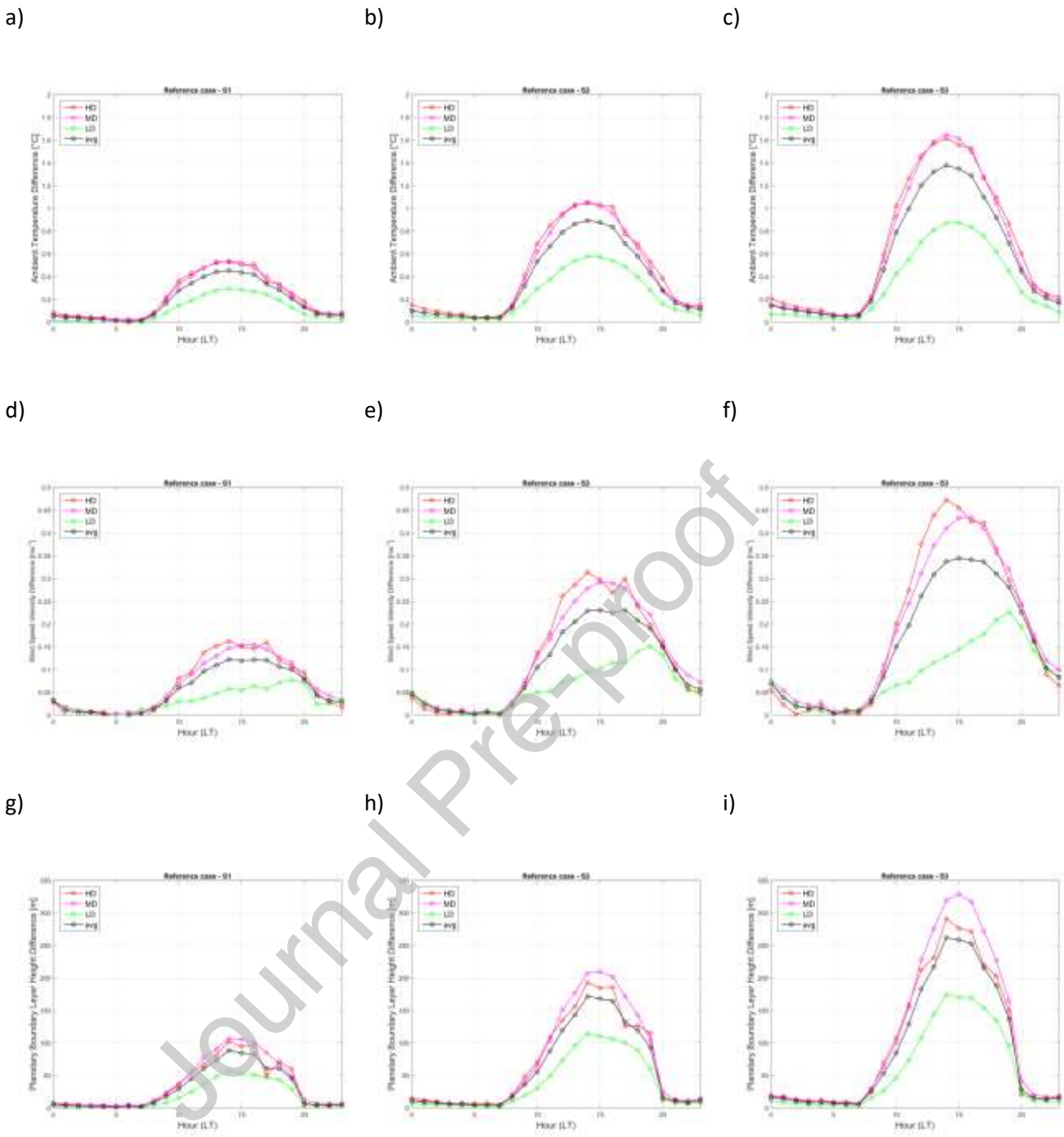

Figure 6. Same as Figure 5, but for ambient temperature, wind speed and PBLH.

4.4. Comparison against existing studies

The potential decrease of the ambient temperature because of the urban albedo increase is evaluated for many cities using mesoscale and microscale numerical modeling. An analysis of 30 case studies is provided in Santamouris, 2014a. A second study of similar nature has analyzed

another 14 numerical studies performed mainly under heat wave conditions (Santamouris and Fiorito, 2021). It is concluded that there are very significant differences between the cities in terms of the magnitude of the temperature drop caused by the albedo increase. It is observed that parameters like the level of the urban green infrastructure, the percentage of streets and pavements, the urban population and the urban density determine at large the levels of temperature drop (Santamouris and Fiorito, 2021). Although the synergies between the climatic impact of modified urban albedo with the above parameters are well documented, it is very convenient to use a simple linear relation between the temperature drop and the increase of the urban albedo like the following one (Santamouris, 2014a; Santamouris and Fiorito, 2021):

$\Delta T_{17} = \alpha\Delta(Alb)$

Where ΔT_{17} is the temperature drop of the afternoon daily temperature (at 17:00 LT) caused by the modification of the urban albedo, while Δ(Alb) is the considered change of the mean albedo and α is a coefficient. Based on the data of 30 case studies reported in (Santamouris, 2014a), the coefficient α is equal to α =3.1, while a much lower value, α =1.8 is calculated using the 14 case studies (Santamouris and Fiorito, 2021). The average temperature drop in Melbourne as calculated for the three albedo scenarios corresponds to a value close to α =2.31 and lies between the range proposed by the previous studies. The temperature drop slope for the low density parts of the city are slightly lower than the proposed association in (Santamouris and Fiorito, 2021), while for the average and high density zones the slope is closer to the figure proposed in (Santamouris, 2014a) (Figure 7). When new data calculated for Melbourne and also for Dubai are added in the association proposed by (Santamouris and Fiorito, 2021), the slope is increasing to α=2.016, close to the Melbourne data.

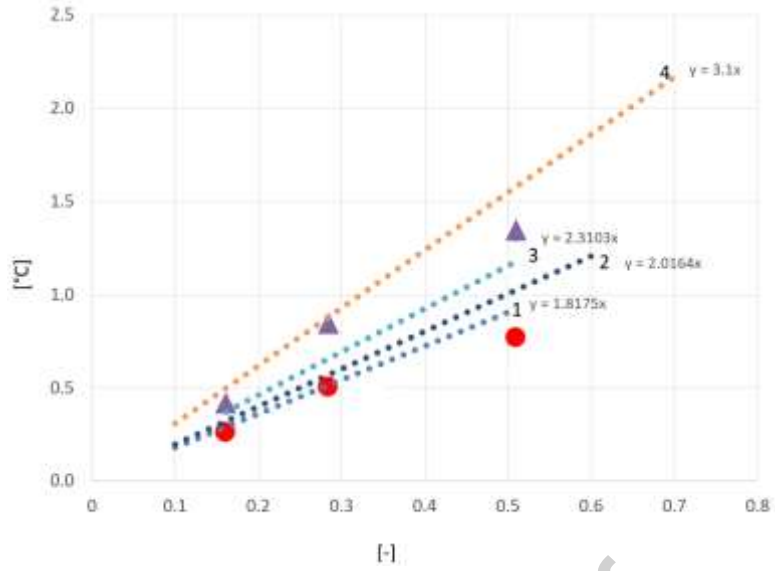

Figure 7. Association of the albedo increase and the corresponding temperature drop at 17:00 LT : (1) As proposed by (Santamouris and Fiorito, 2021), (2) As proposed by (Santamouris and Fiorito, 2021) including data from Dubai and Melbourne, (3) Present study average values, (4) As proposed by (Santamouris, 2014a). Circles and triangles represent the temperature decrease in low and high density zones of Melbourne.

Conclusions

This paper aims at demonstrating the impact of city scale application of cool materials in terms of mitigation potential and alteration of the local climate. The study has been carried out for the metropolitan area of Melbourne using WRF, a well-established mesoscale numerical weather prediction model. It has pioneering ambitions because of the dimension and the climate of the metropolis: costal oceanic temperate and surrounded by the desert. The modeling results have been compared with air temperature and wind (speed and direction) measurements, acquired in different zones of the city. The reference city average albedo was 0.17 rising up to 0.44. This investigation depicts advantages and disadvantages of the use of high albedo materials by investigating the impacts on surface and near-surface quantities for different urbanization density (High, Middle and Low Density). The mitigation potential for ambient temperature peaking 1.6°C

in the middle and high density classes is impressive considering that only conventional materials were considered in this analysis, while higher performing materials are quickly emerging. Some general considerations can be deduced, while other outcomes are specific to the metropolitan area of Melbourne. Consistently with other studies, benefits in the thermal stress are partly countered by the change of the PBL that may create favorable conditions for stagnation and increase of pollution risks. For ozone in particular, the risk increases due to the reflections of solar radiation. Reductions in the analyzed quantities are maximum in the central hours of the day and minimum (even negligible) during the night and the magnitude of the reductions growths with the increase of the average albedo, from scenario S1 to scenario S3. Results also highlight the role of the breeze transport in extending the thermal benefit of the high albedo materials outside the metropolitan area of Melbourne. In the central hours of the day, the wind blowing from the sea towards the city (and the hinterland) entails that the thermal benefits of this mitigation technique regards also zones not actually affected by the intervention. At the same time, since the sea breeze plays a key-role also in the pollutants transport outside the urban area, its weakening due to high albedo materials negatively affects local air quality (if emissions are not reduced) and pedestrians comfort. The analysis of the results based on an urban density classification points out also the role of the extent of urban surfaces (covered by high albedo materials) in the effectiveness of the high albedo materials. The HD class thus results to have the highest thermal benefit together with the most important side effects in terms of stagnation and poor mixing. Also the so-called "border effect" has been revealed, consisting in the fact that the effectiveness of the high albedo materials in an urbanization class is influenced by the land use of the adjacent cells. The implementation of these materials thus requires a specific assessment for the chosen city, strictly correlated to its morphology, geographical position and emissions sources. The implications associated with the albedo modifications run at several levels and this study proves

the need of implementing adequate metrics, able to encompass the different impacts and, thus, identify the optimum levels for the specific city. Finally, the specificity of the results with respect to the category of urban density invites to consider the differentiation of the scenarios among the classes of urbanization for future development of the work.

Acknowledgements

We are grateful to Alberto Martilli for his support with WUDAPT. The computational resources were provided by CINECA. We acknowledge the CINECA award under the ISCRA initiative, for the availability of high-performance computing resources and support. S. F. was funded by the project RAFAEL code ARS01_00305 - PON R&I 2014-2020, the project RHAPS code 2017MSN7M8 - PRIN 2017 and partially by PON funds "Research and Innovation" 2014-2020, all from the Italian Ministry University and Research (MUR).

Conflict of Interest

The authors declare that there is no conflict of interest.

References

Akbari, H., Cartalis, C., Kolokotsa, D., Muscio, A., Pisello, A. L., Rossi, F., Santamouris, M., Synnef, A., Wong, N. H., & Zinzi, M. (2015). Local climate change and urban heat island mitigation techniques – the state of the art. JOURNAL OF CIVIL ENGINEERING AND MANAGEMENT, 22(1), 1–16. https://doi.org/10.3846/13923730.2015.1111934

Alchapar, N. L., & Correa, E. N. (2016). The use of reflective materials as a strategy for urban cooling in an arid “OASIS” city. Sustainable Cities and Society, 27, 1–14. https://doi.org/10.1016/j.scs.2016.08.015

Andreou, E. (2014). The effect of urban layout, street geometry and orientation on shading conditions in urban canyons in the Mediterranean. Renewable Energy, 63, 587–596. https://doi.org/10.1016/j.renene.2013.09.051

Arrieta, F. R. P., & Lora, E. E. S. (2005). Influence of ambient temperature on combined-cycle power-plant performance. Applied Energy, 80(3), 261–272. https://doi.org/10.1016/j.apenergy.2004.04.007

Brousse, O., Martilli, A., Foley, M., Mills, G., & Bechtel, B. (2016). WUDAPT, an efficient land use producing data tool for mesoscale models? Integration of urban LCZ in WRF over Madrid. Urban Climate, 17, 116–134. https://doi.org/10.1016/j.uclim.2016.04.001

Carnielo, E., & Zinzi, M. (2013). Optical and thermal characterisation of cool asphalts to mitigate urban temperatures and building cooling demand. Building and Environment, 60, 56–65. https://doi.org/10.1016/j.buildenv.2012.11.004

Ching, J., Mills, G., Bechtel, B., See, L., Feddema, J., Wang, X., Ren, C., Brousse, O., Martilli, A., Neophytou, M., Mouzourides, P., Stewart, I., Hanna, A., Ng, E., Foley, M., Alexander, P., Aliaga, D., Niyogi, D., Shreevastava, A., ... Theeuwes, N. (2018). Wudapt: An urban weather, climate, and environmental modeling infrastructure for the anthropocene. Bulletin of the American Meteorological Society, 99(9), 1907–1924. https://doi.org/10.1175/BAMS-D-16-0236.1

Ciancio, V., Salata, F., Falasca, S., Curci, G., Golasi, I., & de Wilde, P. (2020). Energy demands of buildings in the framework of climate change: An investigation across Europe. Sustainable Cities and Society, 60, 102213. https://doi.org/10.1016/j.scs.2020.102213

Coutts, A. M., Daly, E., Beringer, J., & Tapper, N. J. (2013). Assessing practical measures to reduce urban heat: Green and cool roofs. Building and Environment, 70, 266–276. https://doi.org/10.1016/j.buildenv.2013.08.021

Croce, S., & Vettorato, D. (2021). Urban surface uses for climate resilient and sustainable cities: A catalogue of solutions. Sustainable Cities and Society, 75, 103313. https://doi.org/10.1016/j.scs.2021.103313

Dimoudi, A., Zoras, S., Kantzioura, A., Stogiannou, X., Kosmopoulos, P., & Pallas, C. (2014). Use of cool materials and other bioclimatic interventions in outdoor places in order to mitigate the urban heat island in a medium size city in Greece. Sustainable Cities and Society, 13, 89–96. https://doi.org/10.1016/j.scs.2014.04.003

Epstein, S. A., Lee, S.-M., Katzenstein, A. S., Carreras-Sospedra, M., Zhang, X., Farina, S. C., Vahmani, P., Fine, P. M., & Ban-Weiss, G. (2017). Air-quality implications of widespread adoption of cool roofs on ozone and particulate matter in southern California. Proceedings of the National Academy of Sciences, 114(34), 8991–8996. https://doi.org/10.1073/pnas.1703560114

Falasca, S., Ciancio, V., Salata, F., Golasi, I., Rosso, F., & Curci, G. (2019). High albedo materials to counteract heat waves in cities: An assessment of meteorology, buildings energy needs and pedestrian thermal comfort. Building and Environment, 163, 106242. https://doi.org/10.1016/j.buildenv.2019.106242

Falasca, S., Curci, G., & Salata, F. (2021a). On the association between high outdoor thermo-hygrometric comfort index and severe ground-level ozone: A first investigation. Environmental Research, 195, 110306. https://doi.org/10.1016/j.envres.2020.110306

Falasca, S., Gandolfi, I., Argentini, S., Barnaba, F., Casasanta, G., Di Liberto, L., Petenko, I., & Curci, G. (2021b). Sensitivity of near-surface meteorology to PBL schemes in WRF simulations in a port-industrial area with complex terrain. Atmospheric Research, 264, 105824. https://doi.org/10.1016/j.atmosres.2021.105824

Founda, D., & Santamouris, M. (2017). Synergies between urban heat island and heat waves in athens (Greece), during an extremely hot summer(2012). Scientific Reports, 7(1), 10973. https://doi.org/10.1038/s41598-017-11407-6

Freitas, E. D., Rozoff, C. M., Cotton, W. R., & Dias, P. L. S. (2007). Interactions of an urban heat island and sea-breeze circulations during winter over the metropolitan area of São Paulo, Brazil. Boundary-Layer Meteorology, 122(1), 43–65. https://doi.org/10.1007/s10546-006-9091-3

Gosling, S. N., Lowe, J. A., McGregor, G. R., Pelling, M., & Malamud, B. D. (2009). Associations between elevated atmospheric temperature and human mortality: A critical review of the literature. Climatic Change, 92(3–4), 299–341. https://doi.org/10.1007/s10584-008-9441-x

Imran, H. M., Kala, J., Ng, A. W. M., & Muthukumaran, S. (2018). Effectiveness of green and cool roofs in mitigating urban heat island effects during a heatwave event in the city of Melbourne in southeast Australia. Journal of Cleaner Production, 197, 393–405. https://doi.org/10.1016/j.jclepro.2018.06.179

Jacobs, S. J., Gallant, A. J. E., Tapper, N. J., & Li, D. (2018). Use of cool roofs and vegetation to mitigate urban heat and improve human thermal stress in melbourne, australia. Journal of Applied Meteorology and Climatology, 57(8), 1747–1764. https://doi.org/10.1175/JAMC-D-17-0243.1

Johnson, H., Kovats, R.S., McGregor, G., Stedman, J., Gibbs, M., Walton, H., et al. The impact of the 2003 heat wave on mortality and hospital admissions in England. Health statistics quarterly / Office for National Statistics. 2005;(25):6-1

Johnston, F. H., Borchers-Arriagada, N., Morgan, G. G., Jalaludin, B., Palmer, A. J., Williamson, G. J., & Bowman, D. M. J. S. (2021). Unprecedented health costs of smoke-related PM2.5 from the 2019–20 Australian megafires. Nature Sustainability, 4(1), 42–47. https://doi.org/10.1038/s41893-020-00610-5

Khan, H. S., Santamouris, M., Paolini, R., Caccetta, P., & Kassomenos, P. (2021). Analyzing the local and climatic conditions affecting the urban overheating magnitude during the Heatwaves (Hws) in a coastal city: A case study of the greater Sydney region. Science of The Total Environment, 755, 142515. https://doi.org/10.1016/j.scitotenv.2020.142515

Martilli, A., Brousse, O., Ching, J., 2016. Urbanized WRF modeling using WUDAPT. http//www.wudapt.org/wp-content/uploads/2016/05/ Urban. March2016.pdf, (March). pp. 1–8.

Martilli, A., Clappier, A., & Rotach, M. W. (2002). An urban surface exchange parameterisation for mesoscale models. Boundary-Layer Meteorology, 104(2), 261–304. https://doi.org/10.1023/A:1016099921195

National Centers for Environmental Prediction/National Weather Service/NOAA/U.S. Department of Commerce (2015), NCEP GDAS/FNL 0.25 Degree Global Tropospheric Analyses and Forecast Grids, https://doi.org/10.5065/D65Q4T4Z, Research Data Archive at the National Center for Atmospheric Research, Computational and Information Systems Laboratory, Boulder, Colo. (Updated daily.) Accessed 28 Sept 2021.

Pearce, J. L., Beringer, J., Nicholls, N., Hyndman, R. J., & Tapper, N. J. (2011). Quantifying the influence of local meteorology on air quality using generalized additive models. Atmospheric Environment, 45(6), 1328–1336. https://doi.org/10.1016/j.atmosenv.2010.11.051

Peron, F., De Maria, M. M., Spinazzè, F., & Mazzali, U. (2015). An analysis of the urban heat island of Venice mainland. Sustainable Cities and Society, 19, 300–309. https://doi.org/10.1016/j.scs.2015.05.008

Qin, Y. (2015). Urban canyon albedo and its implication on the use of reflective cool pavements. Energy and Buildings, 96, 86–94. https://doi.org/10.1016/j.enbuild.2015.03.005

Ribeiro, I., Martilli, A., Falls, M., Zonato, A., & Villalba, G. (2021). Highly resolved WRF-BEP/BEM simulations over Barcelona urban area with LCZ. Atmospheric Research, 248, 105220. https://doi.org/10.1016/j.atmosres.2020.105220

Ryan, R. G., Silver, J. D., & Schofield, R. (2021). Air quality and health impact of 2019–20 Black Summer megafires and COVID-19 lockdown in Melbourne and Sydney, Australia. Environmental Pollution, 274, 116498. https://doi.org/10.1016/j.envpol.2021.116498

Salata, F., Golasi, I., Petitti, D., de Lieto Vollaro, E., Coppi, M., & de Lieto Vollaro, A. (2017). Relating microclimate, human thermal comfort and health during heat waves: An analysis of heat island mitigation strategies through a case study in an urban outdoor environment. Sustainable Cities and Society, 30, 79–96. https://doi.org/10.1016/j.scs.2017.01.006

Santamouris, M. (2014a). Cooling the cities – A review of reflective and green roof mitigation technologies to fight heat island and improve comfort in urban environments. Solar Energy, 103, 682–703. https://doi.org/10.1016/j.solener.2012.07.003

Santamouris, M. (2014b). On the energy impact of urban heat island and global warming on buildings. Energy and Buildings, 82, 100–113. https://doi.org/10.1016/j.enbuild.2014.07.022

Santamouris, M. (2015). Analyzing the heat island magnitude and characteristics in one hundred Asian and Australian cities and regions. Science of The Total Environment, 512–513, 582–598. https://doi.org/10.1016/j.scitotenv.2015.01.060

Santamouris, M. (2020). Recent progress on urban overheating and heat island research. Integrated assessment of the energy, environmental, vulnerability and health impact. Synergies with the global climate change. Energy and Buildings, 207, 109482. https://doi.org/10.1016/j.enbuild.2019.109482

Santamouris, M., & Chrisomalidou, N. (2001). Energy and Climate in the Urban Built Environment, (Editor). James and James Science Publishers, London.

Santamouris, M., & Fiorito, F. (2021). On the impact of modified urban albedo on ambient temperature and heat related mortality. Solar Energy, 216, 493–507. https://doi.org/10.1016/j.solener.2021.01.031

Santamouris, M., & Kolokotsa, D. (2015). On the impact of urban overheating and extreme climatic conditions on housing, energy, comfort and environmental quality of vulnerable population in Europe. Energy and Buildings, 98, 125–133. https://doi.org/10.1016/j.enbuild.2014.08.050

Santamouris, M., & Yun, G. Y. (2020). Recent development and research priorities on cool and super cool materials to mitigate urban heat island. Renewable Energy, 161, 792–807. https://doi.org/10.1016/j.renene.2020.07.109

Santamouris, M., Cartalis, C., Synnefa, A., & Kolokotsa, D. (2015). On the impact of urban heat island and global warming on the power demand and electricity consumption of buildings—A review. Energy and Buildings, 98, 119–124. https://doi.org/10.1016/j.enbuild.2014.09.052

Santamouris, M., Ding, L., Fiorito, F., Oldfield, P., Osmond, P., Paolini, R., Prasad, D., & Synnefa, A. (2017). Passive and active cooling for the outdoor built environment – Analysis and assessment of the cooling potential of mitigation technologies using performance data from 220 large scale projects. Solar Energy, 154, 14–33. https://doi.org/10.1016/j.solener.2016.12.006

Schinasi, L. H., Benmarhnia, T., & De Roos, A. J. (2018). Modification of the association between high ambient temperature and health by urban microclimate indicators: A systematic review and meta-analysis. Environmental Research, 161, 168–180. https://doi.org/10.1016/j.envres.2017.11.004

Shahidan, M. F., Jones, P. J., Gwilliam, J., & Salleh, E. (2012). An evaluation of outdoor and building environment cooling achieved through combination modification of trees with ground materials. Building and Environment, 58, 245–257. https://doi.org/10.1016/j.buildenv.2012.07.012

Shen, L., Sun, J., & Yuan, R. (2018). Idealized large-eddy simulation study of interaction between urban heat island and sea breeze circulations. Atmospheric Research, 214, 338–347. https://doi.org/10.1016/j.atmosres.2018.08.010

Shooshtarian, S., Rajagopalan, P., & Sagoo, A. (2018). A comprehensive review of thermal adaptive strategies in outdoor spaces. Sustainable Cities and Society, 41, 647–665. https://doi.org/10.1016/j.scs.2018.06.005

Skamarock, W. C., J. B. Klemp, J. Dudhia, D. O. Gill, Z. Liu, J. Berner, W. Wang, J. G. Powers, M. G Duda, D. M. Barker, and X.-Y. Huang, 2019: A Description of the Advanced Research WRF Version 4. NCAR Tech. Note NCAR/TN-556+STR.

Stewart, I. D., & Oke, T. R. (2012). Local climate zones for urban temperature studies. Bulletin of the American Meteorological Society, 93(12), 1879–1900. https://doi.org/10.1175/BAMS-D-11-00019.1

Stewart, I. D., Oke, T. R., & Krayenhoff, E. S. (2014). Evaluation of the 'local climate zone' scheme using temperature observations and model simulations: EVALUATION OF THE 'LOCAL CLIMATE ZONE' SCHEME. International Journal of Climatology, 34(4), 1062–1080. https://doi.org/10.1002/joc.3746

Stull, R. B. (A c. Di). (1988). An introduction to boundary layer meteorology. Springer Netherlands. https://doi.org/10.1007/978-94-009-3027-8

Taleghani, M., Sailor, D. J., Tenpierik, M., & van den Dobbelsteen, A. (2014). Thermal assessment of heat mitigation strategies: The case of portland state university, oregon, usa. Building and Environment, 73, 138–150. https://doi.org/10.1016/j.buildenv.2013.12.006

Tsoka, S., Theodosiou, T., Tsikaloudaki, K., & Flourentzou, F. (2018). Modeling the performance of cool pavements and the effect of their aging on outdoor surface and air temperatures. Sustainable Cities and Society, 42, 276–288. https://doi.org/10.1016/j.scs.2018.07.016

Xu, T., Sathaye, J., Akbari, H., Garg, V., & Tetali, S. (2012). Quantifying the direct benefits of cool roofs in an urban setting: Reduced cooling energy use and lowered greenhouse gas emissions. Building and Environment, 48, 1–6. https://doi.org/10.1016/j.buildenv.2011.08.011

Xu, X., AzariJafari, H., Gregory, J., Norford, L., & Kirchain, R. (2020). An integrated model for quantifying the impacts of pavement albedo and urban morphology on building energy demand. Energy and Buildings, 211, 109759. https://doi.org/10.1016/j.enbuild.2020.109759